Solsona Espriu, BE.; Garcia, T.; Sanchis Martinez, R.; Soriano Rodríguez, MD.; Moreno, M.; Rodríguez-Castellon, E.; Agouram, S.... (2016). Total oxidation of VOCs on mesoporous iron oxide catalysts: soft chemistry route versus hard template method. The Chemical Engineering Journal and the Biochemical Engineering Journal. 290:273-281. https://doi.org/10.1016/j.cej.2015.12.109

Total oxidation of VOCs on mesoporous iron oxide catalysts: soft chemistry route versus hard template method

B. Solsona[1]*, T. García[2*], R. Sanchis[1], M.D. Soriano[3], M. Moreno[4], E. Rodríguez-Castellón[4], S. Agouram[5], A. Dejoz[1], J.M. López Nieto[3]

[1] Departament d´Enginyeria Química, Universitat de València, C/ Dr. Moliner 50, 46100 Burjassot, Valencia, Spain. Email: benjamin.solsona@uv.es

[2] Instituto de Carboquímica (CSIC), C/Miguel Luesma 4, 50018 Zaragoza, Spain. Email: tomas@icb.csic.es

[3] Instituto de Tecnología Química (UPV-CSIC), Campus de la Universidad Politécnica de Valencia, 46022 Valencia, Spain

[4] Department of Inorganic Chemistry, Facultad de Ciencias, Universidad de Málaga, 29071 Málaga, Spain.

[5] Department of Applied Physics and Electromagnetism, Universitat de València, C/Dr. Moliner 50, 46100 Burjassot, Valencia, Spain

* To whom correspondence should be addressed

Abstract

The total oxidation of two representative VOCs, propane and toluene, has been studied using mesoporous α-Fe_2O_3 catalysts. Different preparation methods have been followed leading to mesoporous materials with different characteristics. Whilst a mesoporous catalyst formed by aggregation of nanocrystals has been produced by soft chemistry using oxalic acid as precipitating agent, a mesoporous material with crystalline walls have been prepared by a nanocasting route using a hard template. These catalysts have been characterized by several physicochemical techniques: XRD, N_2 adsorption, TPR, XPS, TEM, HR-TEM, SAED and EDX. Among the different α–Fe_2O_3 catalysts synthesized differences not only in the surface area and morphology have been observed but also in the lattice parameter, in the concentration of oxygen defects for VOCs adsorption and in the reducibility. In the case of the toluene oxidation it has been observed that the catalytic activity is highest for the catalysts prepared by a nanocasting route, which presents a very high surface area of 208 m^2 g^{-1}. Conversely, for propane oxidation the most active catalyst resulted to be the mesoporous nanocrystalline catalyst formed by aggregation. In this case, a direct relationship between reducibility and catalytic activity normalized per surface area has been observed. The differences between toluene and propane oxidation can be tentatively ascribed to different reaction mechanisms to be accounted for.

Keywords: propane, toluene, catalytic total oxidation, mesoporous α-Fe_2O_3, Nanocasting.

Introduction

The emission of volatile organic compounds (VOCs) to the environment presents widespread environmental implications. Thus, pollution by VOCs has been related to the photochemical smog and to ozone depletion [1, 2]. Moreover, many VOCs are themselves toxic and/or carcinogenic [3]. Several methods have been developed, the heterogeneous catalytic oxidation being one of the best options, especially if the VOC concentration is low and the process is continuous [4, 5]. This presents several advantages over the typical thermal oxidation process due to the lower temperature required for the elimination of the VOC, such as a lower need for supplementary fuel (cheaper) and lower formation of undesirable by-products.

VOCs involve a large amount of compounds with different chemical functionality which can be emitted from a range of sources. Among them, linear short chain alkanes are some of the most difficult to destroy [6] and aromatics some of the most toxic [7]. One representative hydrocarbon of each group has been selected for the present study, propane and toluene. Propane is emitted to the atmosphere from a variety of sources as LPG vehicles and stationary power sources. Toluene in spite of its toxicity is also abundantly emitted to the atmosphere as is a very common solvent and also as a reactant in industrial processes.

Although platinum and palladium based catalysts are currently the most efficient for the total oxidation of hydrocarbons [8], the use of metal oxides of non-noble metal offer considerable economic advantages in terms of operating costs, and the level of environmental protection provided [9]. Cobalt oxide, manganese oxide but also iron oxide [10, 11, 12] constitute an alternative to platinum group metal based catalysts. Unfortunately, the activity of these catalysts is in most cases lower and the deactivation important. Although the iron oxide is less active than either cobalt or manganese oxide, it presents a high sintering temperature which can avoid deactivation. Iron oxide presents some additional advantages as it is readily available, environmentally friendly and very cheap.

Bulk iron oxide has been shown as an interesting option for total methane oxidation although it could deactivate due to sintering. The control of the iron oxide calcination temperature is of paramount importance as high calcination temperature usually leads to very poor catalytic performance in terms of both activity and stability. [13]. Thus working at 600ºC a remarkable drop in the hydrocarbon conversion with the time on line is reported. In terms of activity, it is reported that the reaction rate for methane oxidation linearly depends on the amount of iron, suggesting that different iron oxide species and iron oxides with distinct crystallite size presents a very similar intrinsic reactivity [14]. Similarly, the total oxidation of lower alkanes has also been studied using iron oxide catalysts [12, 15], showing that iron oxide was fairly active for the oxidation of propane and propene at low temperatures although less than manganese oxide [15, 16]. Propane presents the advantage over methane of being much more reactive and then the temperature required for activation is remarkably lower. This way, the deactivation by sintering is expected to be minimized.

Additionally, mesoporous iron oxides have been also studied for the destruction of VOCs due to their unique physicochemical properties. Indeed, Xia et al [17] have demonstrated that 3D ordered and wormhole-like mesoporous iron oxide catalysts with a rhombohedral crystal structure have a remarkable activity for the removal of acetone and methanol. High surface area, low-temperature reducibility, high oxygen adspecies concentration and 3D mesoporous structure, are accounted for the good catalytic performance. While there is no doubt about the esthetical appeal of symmetry, it can be observed that periodic and ordered mesoporous catalysts are not offering specific advantages for VOCs total oxidation since the non-ordered mesoporous catalysts prepared by a modified citric acid-complexing method outperform to the ordered mesoporous iron oxides produced using the KIT-6-templating, in agreement with a higher surface area and a lower reducibility observed for the non-ordered catalysts. Against this background, it is worth commenting that the same trend observed for these two catalytic

systems in terms of surface area, catalyst reducibility and catalytic activity prevents a proper elucidation about the influence of each of these parameters on the catalyst performance. Herein, we demonstrate that the role of these parameters is strongly depending on the nature of the organic compound and different descriptors defining the catalytic combustion of dissimilar VOCs should be selected. For this aim, several bulk iron oxide catalysts have been prepared, including a nanocrystalline iron oxide, a mesoporous iron oxide formed by aggregation of nanocrystals and a mesoporous nanocasted material with crystalline walls. All these catalysts have been studied for the total oxidation of two different VOCs, propane and toluene.

2. Experimental

2.1. Preparation of bulk iron oxide catalysts

The nomenclature and some characteristics of the catalysts are detailed in Table 1.

Fe-0 is a commercial Fe_2O_3 supplied from Panreac and calcined at 500ºC for 4 h.

Fe-A was synthesized by dissolving iron (II) nitrate (Fluka, purity > 98%) in deionised water. This solution was evaporated, dried overnight at 120ºC and finally calcined in static air at 500ºC for 4 h.

The mesoporous catalyst formed by aggregation of iron oxide nanocrystals, *Fe-B,* was prepared by mixing in water iron nitrate and oxalic acid (molar ratio= 1:5) and heating at 80ºC until most of water has evaporated. The solid was dried overnight at 120ºC and calcined in static air in two steps, 2 h at 300ºC and 2h at 500ºC.

Fe-C was prepared by a nanocasting route using mesoporous silica with a KIT-6 structure as a hard template. KIT-6 was prepared according to [18, 19] using an autoclave heated at 80ºC. The iron oxide replica was prepared by dispersing the siliceous KIT-6 in ethanol with iron nitrate [20]. After 30 minutes of stirring, the ethanol was removed by evaporation through

heating the mixture for 16 h at 120 ºC in an oven. The resulting powder was heated in a ceramic crucible in an oven at 350 ºC for 6 h to completely decompose the nitrate species. The impregnation step was repeated with a further 5.0 mL of the metal salt in ethanol solution in order to achieve higher iron loadings. After evaporation of the solvent, the resulting material was calcined at 500ºC for 6 h. Finally, the silica template was removed by treatment using 2 M NaOH aqueous solution at 80 °C. The NaOH etching of the silica template was repeated 3 times, each time a fresh 5 mL portion of NaOH solution was used for 2 h. The FeOx catalyst was recovered by centrifugation, washed with water and finally dried at 200 ºC. Finally, a mesoporous iron oxide catalyst with crystalline walls, *Fe-D*, was prepared similarly as in refs [21, 22]. Specifically it was synthesized as follows: 4.5 grams of iron (II) nitrate (Fluka, purity > 98%) were dissolved in 60 mL of ethanol and then it is added 3 gram of dry mesoporous silica KIT-6. The mixture was then stirred at room temperature until a fine and dry powder was obtained. This powder was calcined at 500ºC with a rate of 0.5ºC/min and kept at that temperature for 6 h. The calcined sample was treated with hot 2M NaOH to remove the silica KIT-6 and then it was centrifuged, washed with water-ethanol and finally dried in an oven at 100ºC.

22. Characterization techniques

Catalysts were characterized by N_2 adsorption at -196 ºC, using a Micromeritics ASAP 2020 apparatus. Samples were degassed at 150 ºC prior to analysis. From these data, the following textural parameters were calculated: multipoint Brunauer–Emmet–Teller (BET) surface area (S_{BET}) was estimated from the relative pressure range from 0.05 to 0.25. Pore size distribution and mesopore volumes of these materials were analysed using the Barrett–Joyner–Halenda (BJH) method applied to the adsorption branch of the isotherm.

Powder X-ray diffraction was used to identify the crystalline phases present in the catalysts. An Enraf Nonius FR590 sealed tube diffractometer, with a monochromatic $CuK_{\alpha 1}$ source operated at 40 kV and 30 mA was used. XRD patterns were calibrated against a silicon standard and phases were identified by matching experimental patterns to the JCPDS powder diffraction file.

Temperature programmed reduction was performed using a micromeritics Autochem 2910 apparatus with a TCD detector. The reducing gas used was 10 % H_2 in argon with a total flow rate of 50 ml min^{-1} (GHSV *ca.* 8000 h^{-1}). The temperature range explored was from room temperature to 900 ^{o}C with a heating rate of 10 ^{o}C min^{-1}.

Morphological and structural characterization of the samples was performed by Transmission Electron Microscopy (TEM), high resolution TEM (HRTEM) and selected Area electron diffraction (SAED) by using a FEI Field Emission Gun (FEG) TECNAI G2 F20 S-TWIN microscope operated at 200 kV. Energy Dispersive x-rays Spectroscopy (EDS) in TEM nanoproble mode was achieved to prove the purity of the synthetized iron oxide nanoparticles. The synthesized iron oxide powder samples were treated by sonicating in absolute ethanol for few minutes, and a drop of the resulting suspension were deposited onto a holey-carbon film supported on a copper grid, which was subsequently dried.

The XPS data were collected using a Physical Electronics PHI 5700 spectrometer with non-monochromatic Mg-Kα radiation (300 W, 15 kV, 1253.6 eV) for the analysis of the core level signals of the elements and with a multichannel detector. Spectra of powdered samples were recorded with the constant pass energy values at 29.35 eV, using a 720 μm diameter analysis area. Under these conditions, the Au 4f7/2 line was recorded with 1.16 eV FWHM at a binding energy of 84.0 eV. The spectrometer energy scale was calibrated using Cu 2p3/2, Ag 3d5/2, and Au 4f7/2 photoelectron lines at 932.7, 368.3, and 84.0 eV, respectively. The PHI ACCESS ESCA-V6.F software package was used for acquisition and data analysis. The

recorded spectra were always fitted using Gauss–Lorentz curves, in order to determine the binding energy of the different elements core levels more accurately.

2.4. Catalyst activity determination

Catalytic activity was measured using a fixed bed laboratory micro-reactor. In the propane oxidation experiments, 250 mg of powdered catalyst was placed in a $^1/_2$" o.d. quartz reactor tube. The reactor feed contained 8000 vppm propane in air with a gas hourly space velocity (GHSV) of 20000 h^{-1}. In the case of toluene oxidation experiments 1000 vppm of toluene in air with a GHSV = 30000 h^{-1} was employed. For both oxidations the reactants and products were analysed by an online gas chromatograph with a thermal conductivity and a flame ionisation detector. Two chromatographic columns were employed: i) Porapak Q (for CO_2 and hydrocarbons) and ii) Molecular Sieve 5A (to separate O_2 and N_2). The temperature range 100-500 ^oC was explored and the reaction temperature was measured by a thermocouple placed in the catalyst bed. The differences between the inlet and outlet concentrations were used to calculate conversion data. In order to corroborate this data the chromatographic area of CO_2 was used as the comparative reference. These two procedures lead us to adjust the carbon balance with an accuracy of ±2% for propane oxidation and ±4% for toluene oxidation. Analyses were made at each temperature until steady state activity was attained (ca. 30 minutes before the first analysis) and the results were averaged. Blank experiments were conducted in an empty reactor until 500ºC, showing negligible conversion.

3. Results

3.1. Characterization of catalysts

Figure 1 shows the adsorption isotherms for the different iron oxide catalysts. Fe-A adsorption isotherm is typical of nanocrystalline materials. The isotherms of Fe-B, Fe-C and

Fe-D catalysts are intermediate between type II and type IV, with different balance contributions between inter- and intra-particle mesoporosity. Indeed, a marginal amount of mesoporosity is observed for the Fe-C sample. A poor replication process is achieved for the Fe-B sample, where the formation of iron oxide nanoparticles seems to be more relevant, as shown later. For Fe-B and Fe-D, the increase in slope at *ca.* 0.4 correspond to capillary condensation, typical of mesoporous materials with intra-particle pore systems, while the further increase at higher relative pressures indicates substantial inter-particle porosity. Intra-particle porosity is more noticeable for the Fe-D sample. Accordingly, the pore size distribution of Fe-B and Fe-D samples shows different profiles. A broader pore size distribution between 4 and 50 nm centrered about 17 nm is observed for the mesoporous sample formed by aggregation of nanoparticles (Fe-B), whilst the nanocasted sample (Fe-D) shows the presence of a narrower BJH pore diameter distribution between 4-15 nm (supplementary information, Figure S-1). For this sample, the maximum adsorption appears around 10 nm. Therefore, the inverse replication process has led to mean pore sizes 2-3 times higher than that expected for a KIT-6 replica, which can be linked to the fact that the formation of crystalline bridges between particles is not completely accomplished. This arrangement could explain the absence of long-range mesostructure ordering observed by low-angle powder X-ray diffraction data for Fe-D sample, see Figure 2.

Table 1 shows the physicochemical characteristics of bulk iron oxide catalysts. Depending on the preparation method, the surface areas of the bulk catalysts vary from 26 $m^2 g^{-1}$ to 208 $m^2 g^{-1}$, in spite of the fact that they have been heat treated at the same temperature. The nanoparticulated catalyst, Fe-A, presents a surface area of 26 $m^2 g^{-1}$ whereas the catalysts prepared using oxalic acid as a swelling agent, Fe-B, shows a notable surface area of 71 $m^2 g^{-1}$ consistent with the presence of mesopores formed by aggregation of iron oxide nanocrystals. The Fe-C catalyst prepared using a nanocasting route has a surface area of 53 $m^2 g^{-1}$. This low

value is again pointing out a partial replication process for this sample. Finally, the Fe-D catalyst presents a remarkable high surface area of 208 m^2 g^{-1}, which is one of the largest values ever reported for mesoporous Fe_2O_3 materials prepared by nanocasting [23]. Mesopore volumes are also reported in Table 1. As expected, Fe-D is the sample with the highest mesopore volume, whilst Fe-B sample shows an intermediate value between those samples produced by nanocasting.

Figures 2 show the wide angle-XRD patterns of the catalysts synthesized. The only iron phase identified in all cases was rhombohedral hematite, α-Fe_2O_3 (JCPDS: 33-0664). No diffraction peaks related to another Fe-containing phase were detected.

Fig 3 shows the TPR profiles for bulk iron oxide catalysts. As it can be seen the shape of the profiles is similar for all of them but reductions take place at different temperatures. Similar total hydrogen consumption values are observed, which are close to the theoretical values (18.9 mmol/g). A first band of medium intensity has been observed with the maximum at 300-370 ºC and a second intense band at 400-600ºC which presents two maxima. These profiles have been related to the following transitions: $3Fe_2O_3 + H_2 \rightarrow 2Fe_3O_4 + H_2O$, $Fe_3O_4 + H_2 \rightarrow 3FeO + H_2O$ and $FeO + H_2 \rightarrow Fe^0 + H_2O$ [24, 25]. In the iron oxide prepared with oxalic acid (Fe-B) and the nanoparticulated iron oxide (Fe-A) the reductions occur at lower temperature whereas in those prepared by nanocasting, reductions shift to higher values, in agreement with the lower distortion of the unit cell observed by TEM as shown later. Thus, the maximum of the first band for Fe-A and Fe-B occurs at about 300ºC whereas for the nanocasted catalysts appear at approximately 370ºC. As can be observed there is not a relationship between surface area of the catalyst and reducibility. Therefore, the role of each of these parameters on the catalyst performance can be separately identified. On the other hand, previous published works have reported that the reduction temperature of the first band (from α-Fe_2O_3 to Fe_3O_4) is strongly influenced by the surface area of the catalyst. Increasing

values of surface area leads to lower reduction temperature [26]. However, a different trend is observed in this work. Remarkably, it is observed that the formation of nanocrystalline bridges between the iron oxide nanoparticles, as those formed in the Fe-D sample, negatively influences the reducibility of the iron species, although a remarkably increase in the surface area is attained.

XPS analyses have been conducted on the iron oxide catalysts (Table 2). It must be indicated that the peaks position of Fe 2p1/2 and Fe 2p3/2 and their satellite peaks, are very sensitive to the oxidation states of the iron. For these samples, Fe 2p photoelectron peaks appeared around 710.8 eV and 724.4 eV with a shake-up satellite peak at 718.8 eV, 8 eV above the Fe2p3/2. Separation of the 2p doublet is 13.6 eV, see Figure 4A. All these features are characteristics of Fe^{3+} in Fe_2O_3 [27, 28].

On the other hand, the O1s peak needs to be deconvoluted into two peaks at binding energies of 529.6 and 531.5 eV (Table 2, figure 4B) because of its asymmetry, indicating the presence of oxygen with at least two different chemical environments. Unfortunately, the assignment of these oxygen species is complex. The binding energy of 529–530 eV, denoted as Oα, is characteristic of the lattice oxygen (O^{2-}), and the binding energy in the region of 531–533 eV, denoted as Oβ, may be assigned to defect oxide or to surface oxygen ions with low coordination. There may be a contribution to the 531–533 eV peak from either surface hydroxyl or carbonate species [29, 30]. Catalysts comprised of nanoparticles or prepared by soft chemistry present a higher proportion of lattice Oα species (87%) than those prepared by using a silica hard template (75-78%), where the relative amount of oxygen defects for VOCs adsorption is higher.

Figure 5 shows representative TEM conventional micrographs of the synthesized iron oxide catalysts. As we can observe in TEM images, the sample Fe-A (Fig. 5 pictures a and e) consists of nanoparticles (NPs) without a well-defined shape and with size ranging from 20 to

50 nm. Sample Fe-B (Figure 5, pictures b and f) presents a completely different aspect as it is formed by the alignment of aggregates of iron oxide nanoparticles; in this case the size of the interconnected nanoparticles is lower. In fact, the analysis of more than 200 NPs showed that the size varies between 20 and 35 nm in diameter; it is also of interest to emphasize that some areas on the material consist of domains of 200x500 nm^2. The Fe-C catalyst shows a significant change in size and morphology of the iron oxide (Fig. 5, pictures c and g), in which two types of structures are observed: i) a partially ordered mesoporous framework composes of small NPs with about 6-8 nm in diameter; the surface of the continued ordered mesostructure area is about 100x100 nm^2, and ii) compact agglomerations composes of randomly distributed NPs with larger size ranging from 20 to 55 nm.

Finally, Fe-D catalyst (Fig.5, pictures d and h) shows an ordered mesoporous structure composes of uniform nanoparticles linked by nanocrystalline bridges. Accordingly, the surface area observed is remarkably larger than that found in sample Fe-C. The average particle size of Fe-D sample (from counting more than 200 particles) is about 7 ± 1 nm, which is similar to that of the smaller NPs synthesized in sample Fe-C. Similarly, the mesopore structure observed in Fe-D is similar to that observed for Fe-C, but in the case of Fe-D there are not apparent agglomerations of nanoparticles as it happens in Fe-C. HRTEM images shows that the ordered Fe_2O_3 nanoparticles with size about 6 nm in diameter are connected with smaller dots as a nanobridge with size about 2-3 nm length.

Both the high-resolution TEM (HRTEM) and the selected area electron diffraction pattern are used to obtain structure information of the synthesized iron oxide nanoparticles. In fact, SAED inserted in Fig. 5a of Fe-A sample shows a characteristic polycrystalline diffraction pattern of particles with well-defined spots distributed in at least seven diffraction rings. The measured interplanar distance determined from electron diffraction pattern from the center to the outer ring are as follow: 3.665, 2.670, 2.535, 2.230, 2.08, 1.71 and 1.471 Å, corresponding

to the planes (110), (120), (-110), (220), (020), (132) and (130), respectively, which are indexed with Fe_2O_3 structure (JCPDS: 85-0599) with space group R-3c÷ and are in good agreement with the XRD measurements. The same trend has been observed for the other iron oxide catalysts studied.

The single crystalline structure of nanoparticles is also confirmed by the high-resolution TEM image, as shown in Fig. 6 for Fe-C and Fe-D catalysts, suggesting the nanoparticles are single crystals as indicated clearly by atomic lattice fringes. Direct measurement of spacing in between the crystal fringes visualizes in the HRTEM micrograph is 3.73 Å (Fig.6a) and corresponding to the (210) lattice spacing of α-Fe_2O_3, another lattice spacing of 2.53 Å (Fig. 6b) between adjacent lattice planes corresponds to the (311) planes of α-Fe_2O_3. Local EDX analysis in nanoprobe mode (spot size of the beam < 5 nm) confirms the composition nature of NP and is composed of O and Fe; and reveals the presence of a small quantity of Si in Fe-C and Fe-D, due to the incomplete silica removal during the preparation method.

The measured a-lattice parameter from HRTEM images and SAED patterns shows a lower value in those catalysts prepared using a hard template and it can be related to the observed decrease in grain size. Fe-D sample consisted of nanoparticles with size about 5-7 nm having a mean lattice parameter of 5.361 Å whereas for Fe-C sample is 5.388 Å. On the other hand samples Fe-A and Fe-B consisting of bigger grains with size ranging from 20 to 50 nm present lattice parameter of 5.406 and 5.414 Å, respectively.

The catalysts have been tested for the oxidation of propane and toluene (Table 3). For all the catalysts the main reaction product is CO_2. In some cases in the propane oxidation low selectivities to propylene are observed which decreased when the conversion increases. We want to note that yields to propylene never exceeded 1%. The existence of traces of carbon monoxide cannot be ruled out.

Figure 7 shows the variation of the propane (Fig. 7a) and toluene (Fig. 7b) conversion with the reaction temperature. A different trend is observed for both hydrocarbons. Thus the mesoporous catalyst with nanocrystalline walls (Fe-D) and the mesopore catalyst formed by aggregation of nanocrystals (Fe-B) are the most active catalyst for the catalytic combustion of toluene and propane, respectively. Sample Fe-C has the lowest activity among the catalysts synthesized; only being better than the commercial iron oxide. The order of activity per gram of catalyst, for toluene oxidation, follows the sequence: Fe-D > Fe-B > Fe-A > Fe-C, whereas for propane oxidation the sequence is Fe-B > Fe-D > Fe-A > Fe-C. Thus, for toluene oxidation, 50% conversion is obtained at 185ºC (on the more ordered catalyst) or at 230ºC (on Fe-C catalyst). Similarly, for propane oxidation, 50% conversion is obtained at 305ºC (on Fe-B catalyst) or at 370ºC (on Fe-C catalyst).

If the activity is normalized per surface area the trend varies depending on the hydrocarbon fed (Table 3). Thus, for propane oxidation the catalysts prepared by nanocasting presented the lowest specific activity and the sequence was: Fe-B ≥ Fe-A > Fe-C ≈ Fe-D. However in the toluene oxidation the activity normalized per surface area unit is not very different among the catalysts, although Fe-D, results to be the most active and the sequence is: Fe-D > Fe-B, Fe-A > Fe-C.

4. Discussion

In the present paper mesoporous α–Fe_2O_3 catalysts have been synthesized. Whilst a mesoporous catalyst formed by aggregation of nanocrystals has been produced using oxalic acid as precipitating agent by a soft chemistry route, a mesoporous material with crystalline walls have been prepared by a nanocasting method. In both cases an activity remarkably higher than either a commercial or nanoparticles of iron oxide has been observed. In fact, the

reaction temperature to obtain a given conversion has decreased in the best cases 125-150ºC compared to the commercial catalyst. The most active catalyst for toluene oxidation has resulted to be the mesoporous α–Fe_2O_3 prepared by a nanocasting route (Fe-D), whereas the most active catalyst for propane oxidation has been the mesoporous catalyst formed by aggregation of nanocrystals (Fe-B).

The different catalytic activity for VOC oxidation can be explained on the basis of several parameters. It is observed that whilst surface area seems to be a key parameter for the catalytic combustion of toluene, this parameter is not a proper descriptor for the total oxidation of propane. Indeed, Fe-B shows catalytic activity in propane oxidation ca. 10 times higher than the nanocast Fe-C catalyst, which presents a comparable surface area. Even more, Fe-B is more active than nanocast Fe-D catalyst, which has a three-fold surface area. As observed by TPR, the mesoporous catalyst with crystalline walls presents the lowest reducibility. Therefore, it can be assumed that the presence of intracrystalline bridges between the iron oxides nanoparticles, as observed by TEM, could stabilize the catalyst surface, leading to the formation of hardly reducible iron species. The specific nature of the active sites responsible for total oxidation of propane in metal oxides is not completely understood; however, the catalytic activity during the deep oxidation of light paraffins, such as propane, is tightly related to the reduction and reoxidation of the active sites of the catalyst. Hence, several authors [31-34] have demonstrated that alkane oxidation on metal oxides takes place via a Mars Van-Krevelen mechanism involving lattice oxygen through a redox cycle. Accordingly, in this work a clear correlation can be established in the total oxidation of propane between reducibility (quantified as the temperature of the maximum of the first reduction band) and catalytic activity normalized per surface area (Fig. 8a), suggesting that the limiting step in the propane oxidation on iron oxides is the reduction step and probing that this reaction proceeds via a lattice oxygen Mars-Van Krevelen mechanism. In fact it is widely

known that for the oxidation of short chain alkanes on metal oxides at temperatures over 250ºC once the adsorption of the hydrocarbon and the reduction of the metal oxide takes place, the subsequent oxidation is usually considerably faster [35].

In the case of toluene oxidation the highest catalytic activity per gram of catalyst has been achieved by the most ordered catalyst, Fe-D, indicating that a different catalytic combustion mechanism can be accounted for this compound. Thus, Fig 8b presents the variation of the activity normalized per surface area and the reducibility of the catalyst, where a lack of correlation is evident. Some minor differences have been appreciated among the distinct catalysts, being the Fe-D catalyst that with the highest reaction rate per surface area unit. This fact could be related to a higher relative amount of oxygen defects for VOCs adsorption as seen by XPS analysis. In agreement with this, Duran et al. [16] proposed that the oxidation of toluene on iron oxide and manganese oxide proceeds via a Rideal-Eley mechanism, in which an adsorbed compound reacts with another reactant which has not been adsorbed on the surface of the catalyst. Therefore, in this case, the importance on catalytic activity of both the surface area and the relative amount of oxygen defects for VOCs adsorption would be high as more adsorption sites would be available whereas the reducibility would not contribute so much. In line with this, Fe-A and Fe-B samples exert lower reaction rate values per surface area unit than Fe-D catalyst since the former samples show lower relative amount of oxygen surface defects than the latter. A comparable relative amount of surface oxygen defects for Fe-A and Fe-B samples could explain their comparable specific activity despite of their different surface areas. A further mechanistic study including the use of transient reactors would be highly interesting as it could corroborate what it is proposed in the present article. Finally, it is worth commenting that according to TEM data, Fe-C sample exhibits a non-homogeneous morphology where bulk iron oxide nanoparticles together with mesoporous ordered nanocrystals are observed. The presence of these nanoparticles could block the

accessibility of the toluene molecules to the adsorption sites, leading to conversion rates lower than those expected theoretically. It cannot completely ruled out that the presence of amorphous silica is also blocking the accessibility to the adsorption sites.

The stability of the most representative catalysts in reaction conditions was studied in propane oxidation. Stability tests were conducted on the most active catalyst synthesized, bulk Fe-B. Figure 9a shows three cycles and apparently no differences could be observed among the results of any of the three cycles, showing an excellent stability. Moreover at a reaction temperature of 275ºC, the catalyst is left for 24 h in the usual reaction conditions for propane oxidation. No fall of activity was observed; likely due to the low reaction temperature used, much lower than that the catalyst had been previously activated. This contrasts with the results reported for methane oxidation [13] where an important deactivation is described. Similarly, the stability of Fe-D catalyst is also demonstrated after 3 cycles in toluene oxidation (Fig. 9b).

We want to remark that during the synthesis procedure of bulk ordered catalysts by nanocasting, sodium, which in many reactions is a poison, has been employed. However we do not think the presence of sodium in the catalysts is the responsible for the low activity as in the preparation method the catalyst was thoroughly washed to remove the possible remaining sodium. In the Fe-D catalyst the absence of sodium has been confirmed by EDX and XPS analysis.

The influence of the preparation method has been shown to be of outstanding importance for the synthesis of catalysts composed only of α–Fe_2O_3. Thus, not only the morphology of the catalyst varies depending on the method employed but also the relative amount of oxygen defects for VOC adsorption and the reducibility of the catalysts for redox reactions. Thus, the catalysts with certain extent of order prepared by a nanocasting route present a low reducibility and consequently low specific activity for propane oxidation. In the case of

toluene oxidation it seems that both a high surface area and a higher relative amount of oxygen defects are the determining parameters.

Overall, a high surface area iron oxide prepared by nanocasting presents a remarkably high catalytic activity in the oxidation of two representative VOCs: propane and toluene. In the case of propane oxidation the nanocasting catalysts present a lower specific and intrinsic rate than a mesoporous iron oxide formed by aggregation of nanocrystals, which must be related to a lower reducibility of iron sites in mesoporous iron oxides with crystalline walls. For the optimization of the catalytic activity an increase in the surface area of the catalyst would be meaningful, although other factors should be also controlled in order to improve the intrinsic activity, such as the reducibility of the iron sites.

Conclusions

A mesoporous iron oxide with crystalline walls has been prepared by nanocasting leading to a remarkable high surface area (208 $m^2 g^{-1}$) that positively affects the catalytic activity in the total oxidation of two representative VOCs: propane (as a model of short chain alkane) and toluene (as a model for an aromatic compound). This catalyst reduces the light off in ca. 150ºC compared to a commercial iron oxide.

Different preparation methods have been followed to synthesize α–Fe_2O_3 catalysts and differences not only in the surface area and morphology have been observed but also in the lattice parameter, in the relative concentration of oxygen defects for VOCs adsorption and in the reducibility. Thus, mesoporous iron oxide with crystalline walls prepared by nanocasting shows a lower lattice parameter, a higher relative concentration of oxygen defects (by XPS) and a lower reducibility that a mesoporous catalyst prepared by aggregation of iron oxide nanocrystallites using the principles of the soft chemistry.

Interestingly, the catalytic activity of the catalysts depends on the hydrocarbon used. Thus, in the case of the toluene oxidation the highest catalytic activity was obtained with the high surface area catalyst prepared by nanocasting, the catalytic activity being roughly proportional to the surface area of the catalysts. Conversely, for propane combustion, this nanocasted catalyst presents high activity but lower than that obtained by a mesoporous iron oxide formed by aggregated nanocrystals and this is related to the different reducibility. In fact, in propane oxidation, a direct relationship between reducibility and catalytic activity normalized per surface area has been observed. The differences between toluene and propane oxidation have been tentatively ascribed to different reaction mechanisms taking place.

Acknowledgments

The authors would like to acknowledge the DGICYT in Spain (CTQ2012-37925-C03-1, CTQ2012-37925-C03-2, CTQ2012-37925-C03-3 and CTQ2012-37984- C02-01) and FEDER for financial support. We also thank the University of Valencia and SCSIE-UV for assistance.

References

[1] M. S. Jennings, M. A. Palazzolo, N. E. Krohn, R. M. Parks, R. S. Berry and K. K. Fidler, Catalytic Incineration for the Control of Volatile Organic Compound Emission, Pollution Technology Review, Noyes Ed., No. 121. (1985).

[2] M.J. Molina and F.S. Rowland, Stratospheric sink for chlorofluoromethanes-chlorine atom catalyzed destruction of ozone, Nature, 249 (1974) 810-812.

[3] Environmental Protection Agency, US Clean Air Act, 1990, USA.

[4] H. Wani, R.M.R. Branion, A.K. Lau, Biofiltration: A Promising and Cost-Effective Control Technology for Odors, VOCs and Air Toxics, J. Environ. Sci. Health, A32(7) (1997) 2027-2055.

[5] VOC control: Technology selection criteria and commercial systems review. Air Poll. Consultant, 5 (1995) 4.1-4.18.

[6] T.V. Choudhary, S. Banerjee, V.R. Choudhary, Catalysts for combusion of methane and lower alkanes, Appl. Catal. A: Gen., 234 (2002) 1-23.

[7] J. E. Germain. (1967), Catalytic Conversion of Hydrocarbons, Academic Press. New York.

[8] K. Everaert and J. Baeyens, Catalytic combustion of volatile organic compounds, J. Hazard. Mater., B 109 (2004) 113-139.

[9] W.B. Li, J.X. Wang and H. Gong, Catalytic combustion of VOCs on non-noble metal catalysts, Catal. Today, 148 (2009) 81-87.

[10] E. Grabowski, M. Guenin, M-C. Marion, M. Primet, Catalytic properties and Surface states of cobalt-containing oxidation catalysts, Appl. Catal., 64 (1990) 209-224.

[11] S.S.T. Bastos, J.J.M. Orfao, M.M.A. Freitas, M.F.R. Pereira, J.L. Figueiredo, Manganese oxide catalysts synthesized by exotemplating for the total oxidation of ethanol, Appl. Catal. B 93 (2009) 30–37.

[12] M. Baldi, V. Sánchez-Escribano, J.M. Gallardo Amores, F. Milella, G. Busca, Characterization of manganese and iron oxides as combustion catalysts for propane and propene, Appl. Catal. B 17 (1998) L175–L182.

[13] A.L. Barbosa, J. Herguido, J. Santamaría, Methane combustion over unsupported iron oxide catalysts, Catal. Today, 64 (2001) 43-50.

[14] V.A. Sazonov, Z.R. Ismagilov, N.A. Prokudina, Catalytic combustion of lean methane–air mixtures, Catal. Today, 47 (1999) 149-153.

[15] T. Kobayashi, N. Guilhaume, J. Miki, N. Kitamura, M. Haruta, In situ Raman spectroscopy. A powerful tool for studies in selective catalytic oxidation, Catal. Today, 32 (1996) 171-175.

[16] F.G. Duran, B.P. Barbero, L.E. Cadus, C. Rojas, M.A. Centeno, J.A. Odriozola, Manganese and iron oxides as combustion catalysts of volatile organic compounds, Appl. Catal. B: Environ. 92 (2009) 194–201.

[17] Y. Xia, H. Dai, H. Jiang, L. Zhang, J. Deng, Y. Liu, Three-dimensionally ordered and wormhole-like mesoporous iron oxide catalysts highly active for the oxidation of acetone and methanol, J. Hazard. Mater., 186 (2011) 84–91.

[18] E. Rossinyol, J. Arbiol, F. Peiró, A. Cornet, J.R. Morante, B. Tian, T. Bob, D. Zhao, Nanostructured metal oxides synthesized by hard template method for gas sensing applications, Sens. Actuators B 109 (2005) 57–63.

[19] B. Puertolas, B. Solsona, S. Agouram, R. Murillo, A.M. Mastral, A. Aranda, S.H. Taylor, T. Garcia, The catalytic performance of mesoporous cerium oxides prepared through a nanocasting route for the total oxidation of naphthalene, Appl. Catal. B: Environ. 93 (2010) 395–405.

[20] T. Garcia, S. Agouram, J.F. Sánchez-Royo, R. Murillo, A.M. Mastral, A. Aranda, I. Vázquez, A. Dejoz, B. Solsona, Deep oxidation of volatile organic compounds using ordered cobalt oxides prepared by a nanocasting route, Appl. Catal. A 386 (2010) 16–27.

[21] F. Jiao, A. Harrison, J-C. Jumas, A.V. Chadwick , W. Kockelmann, P.G. Bruce, Ordered mesoporous Fe2O3 with crystalline walls, J. Am.Chem. Soc. 128 (2006) 5468-5474.

[22] A.H. Lu, D. Zhao, Y. Wan, Nanocasting: A Versatile Strategy for Creating Nanostructured Porous Materials, RSC Nanoscience and Nanotechnology No. 11, 2010.

[23] D. Gu, F. Schuth, Synthesis of non-siliceous mesoporous oxides, Chem. Soc. Rev. 43 (2014) 313-344.

[24] K. Park, J.H. Jung, H. Seo, O. Kwon, Mesoporous silica-pillared Kenyaite and magadiite as catalytic support for partial oxidation of the methane, Microp. Mesop.Mat. 121 (2009) 219–225.

[25] F. G. E. Nogueira, J. H. Lopes, A. C. Silva, R. M. Lago, J. D. Fabris, Luiz, C.A. Oliveira, Catalysts based on clay and iron oxide for oxidation of toluene, Appl. Clay Sci. 51 (2011) 385–389.

[26] S.A.C. Carabineiro, N. Bogdanchikova, P.B. Tavares, J.L. Figueiredo, Nanostructured iron oxide catalysts with gold for the oxidation of carbon monoxide, RSC Adv. 2 (2012) 2957–2965.

[27] A.P. Grosvenor, B.A. Kobe, M.C. Biesinger, N.S. McIntyre, Investigation of multiplet splitting of Fe 2p XPS spectra and bonding in iron compounds, Surface and Interface Analysis 36 (2004) 1564-1574.

[28] T.C. Lin, G. Seshadri, J.A. Kelber, A consistent method for quantitative XPS peak analysis of thin oxide films on clean polycrystalline iron surfaces, Applied Surface Science 119 (1997) 83-92.

[29] A. Galtayries, R. Sporken, J. Riga, G. Blanchard, R. Caudano, XPS comparative study of ceria/zirconia mixed oxides: powders and thin film characterisation, J. Electron Spectrosc. 88 (1998) 951–956.

[30] T.L. Barr, An ESCA study of the termination of the passivation of elemental metals, J. Phys. Chem-US, 82 (1978) 1801–1810.

[31] C. Li, Y. Shen, M. Jia, S. Sheng, M.O. Adebajo, H. Zhu, Catalytic combustion of formaldehyde on gold/iron-oxide catalysts, Catal. Commun. 9 (2008) 355–361.

[32] N. Bahlawaue, Kinetics of methane combustion over CVD-made cobalt oxide catalysts, Appl. Catal. B: Environ. 67 (2006) 168-176.

[33] B. Solsona, T.E. Davies, T. García, I. Vázquez, A. Dejoz, S.H. Taylor, Total oxidation of propane using nanocrystalline cobalt oxide and supported cobalt oxide catalysts, Appl. Catal. B 84 (2008) 176–184.

[34] B. Solsona, M. Pérez-Cabero, I. Vázquez, A. Dejoz, T. García, J. Álvarez-Rodríguez, J. El-Haskouri, D. Beltrán, P. Amorós, Total oxidation of VOCs on Au nanoparticles anchored on Co doped mesoporous UVM-7 silica, Chem. Eng. J. 187 (2012) 391– 400

[35] J. R. Monnier and G.W. Keulks, The catalytic oxidation of propylene. IX. The kinetics and mechanism over β-Bi2Mo2O9, J. Catal. 68 (1981) 51-66.

Caption to figures.

Figure 1. Isotherm linear plot for iron oxide catalysts prepared by different methods.

Figure 2. XRD patterns for iron oxides catalysts. The XRD patterns low angle measured for Fe-D has been also included.

Figure 3. Temperature programmed reduction profile of the differently prepared iron oxide catalysts.

Figure 4. Fe 2p XPS spectra for the iron oxide catalysts synthesized (A) and deconvolution of the O1s signal (B).

Figure 5. Typical low magnification of TEM images of. (a,e) Fe-A, (b,f). Fe-B, (c,g) Fe-C and (d,h) Fe-D. The inset figure in figure (5a) is the corresponding SAED patterns of FeOx.

Figure 6. High resolution images of α-Fe2O3 particles, (a) Fe-C, (b) Fe-D. The inserted figure in (b) is the corresponding EDX spectrum of the selected area.

Figure 7. Variation of the propane (a) and toluene (b) conversion with the reaction temperature for the differently prepared iron oxide catalysts. Symbols: (x) Fe-0, (○) Fe-A, (●) Fe-B, Fe-C (■), Fe-D (□). Note: reaction conditions shown in text.

Figure 8. Variation of the specific activity for propane oxidation (determined at 250ºC) or toluene oxidation (determined at 175ºC) with the temperature of the maximum of the first peak in the TPR profiles. Note: Note: (catalytic activity normalized per surface area) is expressed as 10^5 $g_{hydrocarbon}$ m^{-2} h^{-1}.

Figure 9. Stability tests: a) Variation of Propane conversion with the reaction temperature for Fe-B catalyst; and b) Variation of Toluene conversion with the reaction temperature for Fe-D catalyst. Symbols: (●, ■) 1st cycle, (○, □) 2nd cycle, (●, ■) 3rd cycle. Note: Reaction conditions in text.

Table 1. Physico-chemical characteristics of iron containing catalysts.

Catalyst		Si/Fe[a]	S_{BET}	V_{MESO}	Fe_2O_3 (nm)[b]	TPR results	
		wt.	(m^2/g)	(cm^3/g)		H_2-uptake(mmol/g)	$T_{1st\ max}$ /TMC[c]
Fe-0	Commercial	<0.001	3.3	0.01	61.1	19.07	377/618
Fe-A	Nanoparticles	<0.001	26	0.05	28.6	19.61	315/504
Fe-B	Non ordered	<0.001	71	0.20	11.1	19.02	298/470
Fe-C	Nanocasting low area	0.036	53	0.10	19.5	19.44	370/662
Fe-D	Nanocasting high area	<0.01	208	0.38	Very low	18.61	376/649

[a] Si/Fe ratio in weight due to the non removed silica ; [b] estimated through the XRD patterns by the Scherrer equation; [c] T_{1stmax} stands for the temperature of the 1st maximum and TMC the temperature at which the maximum hydrogen consumption is achieved.

Table 2. XPS analysis of bulk iron oxides.

Sample	Oxygen signals detected O1s			Iron signals detected (eV)	
	Oα (eV)	Oβ (eV)	Oβ/O (%)	2p3/2	satellite
Fe-A	529.6	531.5	13	710.6	718.5
Fe-B	529.8	531.9	13	710.6	718.8
Fe-C	529.6	531.6	22	710.6	718.7
Fe-D	529.8	531.7	25	710.7	719.0

Table 3. Catalytic properties of iron oxide catalysts.

Sample	Toluene oxidation[a]				Propane oxidation[a]				
	T10 / ºC	T50 / ºC	Catalytic activity[b]	Specific activity[c]	T10 / ºC	T50 / ºC	T90 / ºC	Catalytic activity[b]	Specific activity[c]
Fe-0	255	305	-	-	375	> 425	>>425	-	-
Fe-A	190	215	0.96	3.71	275	330	380	2.58	9.92
Fe-B	180	210	2.70	3.80	255	305	350	7.61	10.91
Fe-C	200	230	1.18	2.22	305	370	405	0.86	2.60
Fe-D	155	185	11.46	5.51	265	315	370	5.06	2.43

[a] Reaction conditions detailed in the experimental part. Catalytic activity and specific activity determined at 175ºC for toluene oxidation and at 250ºC for propane oxidation; [b] In $g_{hydrocarbon}\ kg_{cat}^{-1}\ h^{-1}$; [c] specific activity (catalytic activity normalized per surface area) expressed as $10^5\ g_{hydrocarbon}\ m^{-2}\ h^{-1}$.

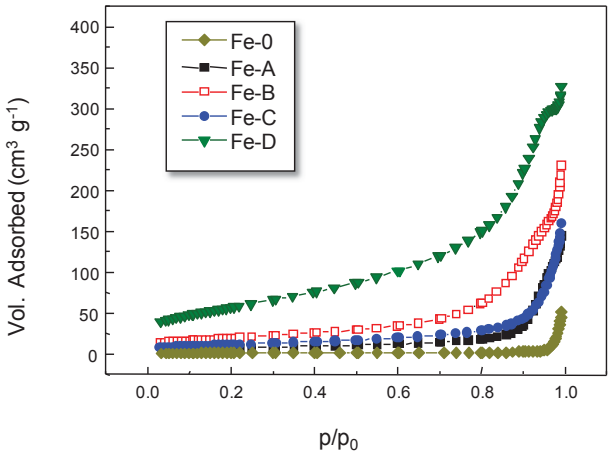
Fe-0
Fe-A
Fe-B
Fe-C
Fe-D
Vol. Adsorbed (cm3 g-1)
p/p0
0
50
100
150
200
250
300
350
400
0.0
0.2
0.4
0.6
0.8
1.0

Figure 1.

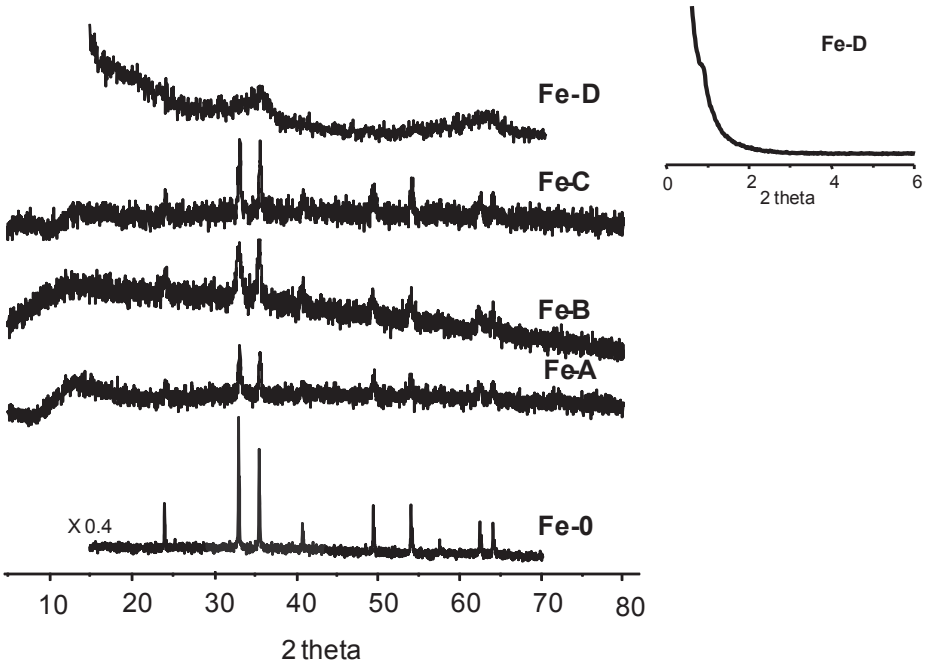
Fe-D
Fe-C
Fe-B
Fe-A
X 0.4
Fe-0
10
20
30
40
50
60
70
80
2 theta
Fe-D
0
2
4
6
2 theta

Figure 2.

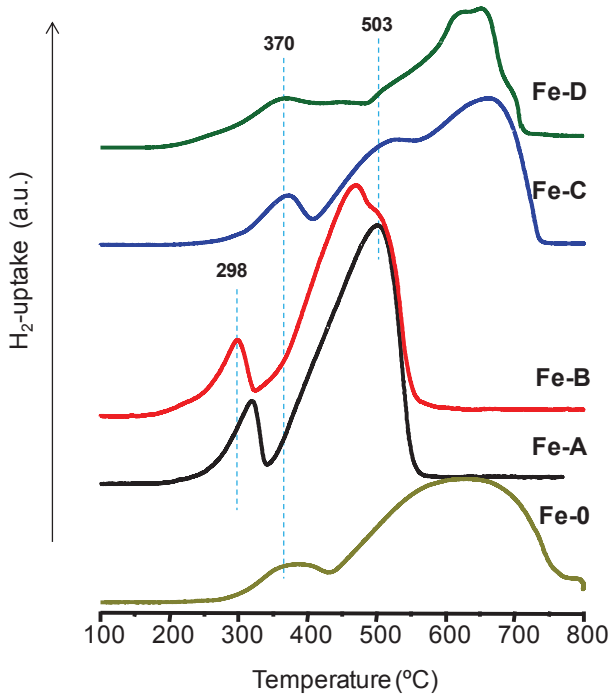
370
503
Fe-D
Fe-C
298
Fe-B
Fe-A
Fe-0
H2-uptake (a.u.)
100 200 300 400 500 600 700 800
Temperature (ºC)

Figure 3.